22nd Australasian Fluid Mechanics Conference AFMC2020
Brisbane, Australia, 7–10 December 2020
https://doi.org/10.14264/8de0a02

Onset of Horizontal Convection

Tzekih Tsai[1] **and Gregory J. Sheard**[1]

[1]The Sheard Lab, Department of Mechanical and Aerospace Engineering
Monash University, Melbourne, Victoria 3800, Australia

Abstract

Horizontal convection describes natural convection flow driven in an enclosure by non-uniform heating imposed across a horizontal boundary. Research has predominantly focused on the dynamics of horizontal convection in thermal equilibrium, where net heat flux through the forcing boundary or any horizontal level in the flow is zero. However, its early transient features and the dynamics of the transition to unsteady flow are not well understood.

The current study numerically investigates the onset of horizontal convection with piecewise constant temperature and uniform heat flux along a bottom boundary of a rectangular enclosure. The onset is found to be characterised by an initial conduction phase followed by a Rayleigh–Bénard type of convection through the thermal boundary layer and finally, bulk overturning flows are established within the enclosure. These regimes and the effects of different heat flux amplitudes and frequencies on the onset of horizontal convection are characterised in the present work.

Keywords
Computational fluid dynamics; Horizontal convection; Heat transfer.

Introduction

Horizontal convection describes convection flow driven in an enclosure by non-uniform heating imposed across a horizontal boundary [4]. These flows are characterised by a Rayleigh number representing the strength of buoyancy over dissipative effects, a Prandtl number and aspect ratio of the enclosure. Numerous studies [2, 8] focused on the dynamics of horizontal convection in thermal equilibrium where no net heat flux through the forcing boundary or through any horizontal level in the flow. The effect of aspect ratio, rotation as well as different temperature profiles on the stability of horizontal convection had been studied by various authors [3, 7, 10]. Local [9] and global [5] linear stability analysis revealed that instability in horizontal convection is due to convective transverse-rolls in the thermal forcing boundary layer. However, the onset of this thermal instability, its early transient features and the dynamics of the transition to unsteady flow are not well understood.

More recently, Sanmiguel Vila *et al.* [6] investigated experimentally the onset of horizontal convection and proposed a scaling for the characteristic time of the transient flow. The current study aims to numerically investigate the onset of horizontal convection. The system considered is similar to the experimental setup used by Sanmiguel vila *et al.* [6]. However, the current investigation expands on the Rayleigh numbers to range from 10^7 to 10^{13}, accounting for the effect of Rayleigh numbers on the onset of horizontal convection.

Numerical Setup

For the study of onset of horizontal convection, the numerical setup consists of a long rectangular tank as depicted in figure 1. The flow is driven by a uniform temperature along the left side (cold) of the enclosure and a uniform heat flux along the right (hot) end of the enclosure. The side and top walls are thermally insulated (zero temperature gradient normal to the walls), and a non-slip condition is imposed on the velocity field on all walls. A Boussinesq approximation for fluid buoyancy is employed, whereby density differences in the fluid are neglected except through the gravity term in the momentum equation. Under this approximation the energy equation reduces to a scalar advection-diffusion equation for temperature which is evolved in conjunction with the velocity field. The fluid temperature is related linearly to the density via thermal expansion coefficient α. In the current study, length, time, velocity, pressure and temperature are respectively non-dimensionalised by L, L^2/κ, κ/L, $\rho_0\kappa^2/L^2$ and $\delta\theta$ (where $\delta\theta$ is a scale for temperature differences based on the input flux and thermal conduction over the length L). The governing equations (conservation of momentum with Boussinesq buoyancy, conservation of mass, and thermal transport) can be written in dimensionless form as

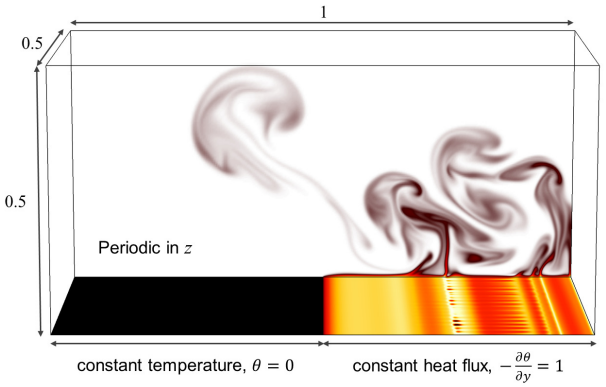

Figure 1. A schematic setup of the computational domain under investigation. The boundary conditions along each of the boundary are as prescribed. Periodic boundary condition is imposed in the out-of-plane direction for three-dimensional simulations. Contours of scalar fields are shown for the heated surface and a z-plane.

$$\frac{\partial \boldsymbol{u}}{\partial t} = -(\boldsymbol{u}\cdot\boldsymbol{\nabla})\boldsymbol{u} - \boldsymbol{\nabla} p + Pr\nabla^2\boldsymbol{u} + PrRa\,\theta\boldsymbol{e}_y, \tag{1}$$

$$\boldsymbol{\nabla}\cdot\boldsymbol{u} = 0, \tag{2}$$

$$\frac{\partial \theta}{\partial t} = -(\boldsymbol{u}\cdot\boldsymbol{\nabla})\theta + \nabla^2\theta, \tag{3}$$

where $\hat{\boldsymbol{e}}_y$ is the unit vector in the y-direction. The horizontal Rayleigh number characterising the ratio of buoyancy to thermal and molecular dissipation is

$$Ra = \frac{g\alpha\delta\theta L^3}{\nu\kappa}, \tag{4}$$

where g is the gravitational acceleration. The Prandtl number characterising the ratio of molecular to thermal diffusion in the fluid is

$$Pr = \nu/\kappa, \tag{5}$$

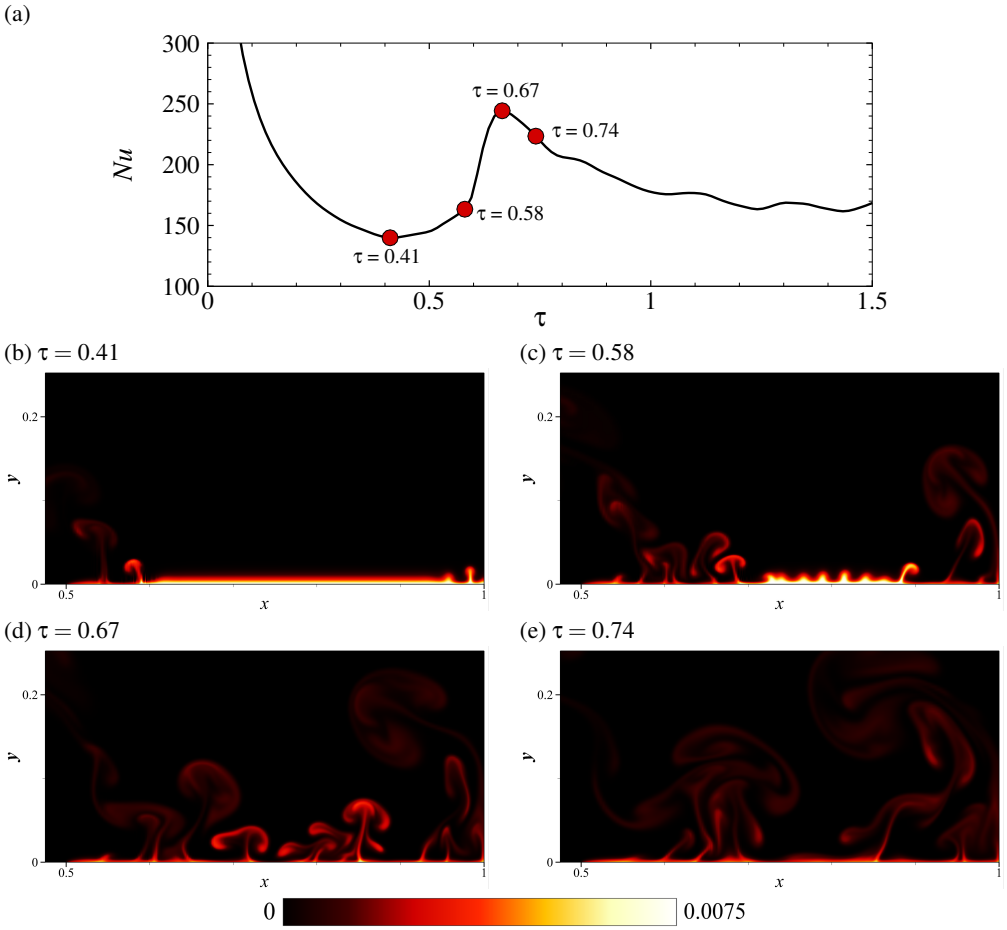

Figure 2. (a) Nusselt number time history with red symbols represent different time instant where snapshot of temperature contours are taken. (b)-(e) Contours plot of temperature field for $Ra_F = 6 \times 10^{11}$ at different time for the onset of horizontal convection as indicated.

and throughout this study $Pr = 6.14$, which approximates water at laboratory conditions (at 25^oC). The Nusselt number characterising the ratio of convective to conductive heat transfer is

$$Nu = \frac{F_\theta L}{\rho_0 c_p \kappa \delta\theta}, \tag{6}$$

where heat flux

$$F_\theta = \kappa \rho_0 c_p \overline{\frac{\partial\theta}{\partial y}}, \tag{7}$$

c_p is the specific heat capacity of the fluid, and $\overline{\partial\theta/\partial y}$ is the averaged absolute vertical temperature gradient along the forcing boundary.

Results and Discussions

Numerical simulations on a rectangular enclosure with an aspect ratio $H/L = 0.5$ and $Pr = 6.14$ were investigated with a fixed cold temperature and a constant heat flux imposed on the left and right half of the enclosure. The system is similar to the experimental setup used by [6]. However, current investigations expand on the Rayleigh numbers to range from 10^6 to 10^{13} to fully account for the effect of Rayleigh numbers on the onset of horizontal convection. The numerical simulation was initialised with a scalar field at the same temperature as imposed along the cold boundary.

Figure 2(a) shows a time history of Nusselt number for $Ra = 6 \times 10^{11}$, the time τ is scaled by a characteristic diffusion time, τ_{bl}, based on the thickness of a thermal boundary layer. At the start of the numerical experiment, the interior temperature was set at the same temperature as the cold boundary, the heat transfer through thermal conduction from the heated boundary into the cold interior. The Nusselt number decreases during the conduction process as heat is transported into the interior. As temperature rises, a thermal boundary layer forms adjacent to the heated boundary. This thermal boundary layer traps heat and eventually leads to plume formation near the centre and the bottom right corner of the enclosure. This can be seen in figure 2(b), which corresponds to the local minimum in the Nusselt number (figure 2(a)). The formation of plumes enhance heat transfer from the heated boundary, thus the Nusselt number begins to rise. As the region of instability in the thermal boundary layer increases, more plumes are formed as shown in figure 2(c). These vertical plumes resemble thermal characteristic of a Rayleigh–Bénard convection [1]. The Nusselt number continues to increase with the formation of more plumes. Figure 2(d) shows the stable thermal boundary layer is completely obliterated by thermal plumes. At this point, the Nusselt number attains its local maximum value which signals the end of the Rayleigh–Bénard convection phase. The effect of the Rayleigh–Bénard convection is to advect heat into the interior through multiple thermal plumes along the heated base. As the plumes rise, horizontal movement of fluid is induced from the cold boundary to replace the rising plumes. This bulk horizontal movement of colder fluid has the effect of stabilising the thermal boundary layer. This can be seen in figure 2 where plumes coalesce and convect toward the right-hand corner of the en-

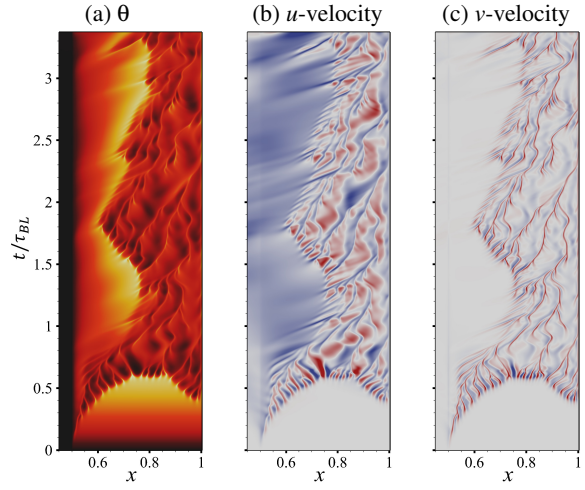

Figure 3. Time evolution of temperature, $u-$ and $v-$velocity fields taken at a height of $y = 0.0015$ inside a thermal boundary layer for $Ra = 6 \times 10^{11}$. The velocity contours range from dark red (negative velocity) to dark blue (positive velocity). The temperature contour levels range from dark to light represent cold and hot temperature respectively.

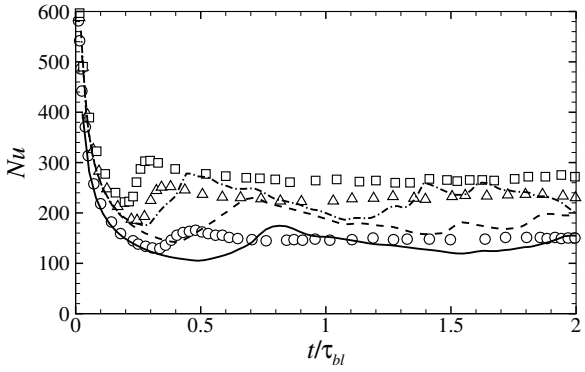

Figure 4. A plot of Nusselt number against time (scaled by the boundary layer diffusion time) for $Ra = 1.6 \times 10^{11}$ (solid line), 6×10^{11} (dashed line) and 1.3×10^{12} (dash-dotted line). Corresponding experimental data from [6] are included for comparison, symbol ◯, △ and □ represent $Ra = 1.6 \times 10^{11}, 6 \times 10^{11}$ and 1.3×10^{12} respectively.

closure, leaving behind fragments of stable thermal boundary layer along the heated boundary. In addition, the plumes are more slanted than before, which is an indicatve of the shear due to the overturning flow established by horizontal convection.

To distinguish between different regimes, the local minimum of the Nusselt number is used to mark the end of conduction regime and the start of the Rayleigh–Bénard convection regime. The local maximum of the Nusselt number represents the end of the Rayleigh–Bénard regime and the beginning of the horizontal convection regime.

The transition between different regimes can be seen visually in figure 3. The figure shows time evolution of temperature, u and v fields taken along a height of $y = 0.0015$ above the heated boundary, it is within the thermal boundary layer. It can be seen from Figure 3(a), initially, the enclosure is heated through conduction where temperature gradually increases from the cold (dark) to hot (yellow). At a scaled time of 0.25, Rayleigh–Bénard plumes begin to appear from the centre of the enclosure. As time increases, more plumes are formed. The horizontal flow over the boundary invoked by the plume eruptions is

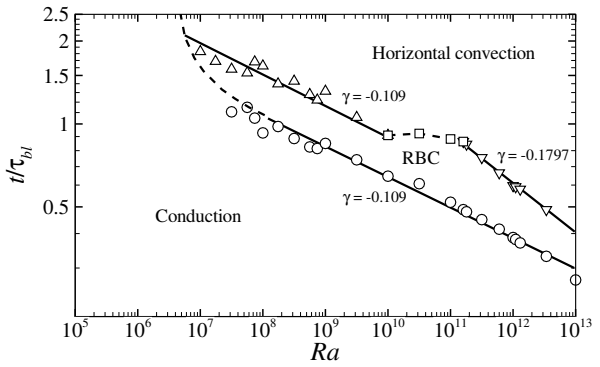

Figure 5. A plot of transition time scaled by the boundary layer diffusion time scale, τ_{bl}, against Rayleigh numbers. The plot shows region of conduction, Rayleigh–Bénard and horizontal convection regimes as a function of Rayleigh number.

revealed by the region of blue shading to the left of figure 3(b). It is apparent that a competition is established between plume eruptions that consume the unstably stratified thermal boundary layer, and the horizontal flow that sweeps the plumes away, permitting the reconstruction of the thermal boundary layer.

Figure 4 shows a time evolution of Nusselt number at three Rayleigh numbers as compared to the experimental results from [6]. The numerical time is scaled by the boundary layer diffusion time scale. The local maximum Nusselt numbers are similar for both experimental and numerical results. However, the local maximum for the numerical simulations are delayed, the duration of which ranges from $t/\tau_{bl} = 0.2$ to 0.4 as the Rayleigh number increases from 1.6×10^{11} to 1.3×10^{12}.

Numerical simulations were conducted for Rayleigh numbers to range from from 10^7 to 10^{13}. Based on the local minimum and maximum Nusselt number, a regime map for the transition between conduction, Rayleigh–Bénard convection and horizontal convection can be obtained as a function of Rayleigh number, as shown in figure 5. It is found that the transition time from conduction to convection scales as $Ra^{-0.109}$. The same scaling is observed for the transition from Rayleigh–Bénard to horizontal convection at $Ra \leq 10^{10}$, whereas a different scaling of -0.1797 is obtained for $Ra \geq 10^{11}$. The regime map indicates the transition time reduces as the Rayleigh number increases and the Rayleigh–Bénard convection is observed prior to the establishment of horizontal convection.

Effect of Imperfections in the Applied Heat Flux

To investigate the possibility of non-uniformity in the experimental conditions [6] as a possible explanation for the observed early onset of horizontal convection, a small sinusoidal variation was introduced to the thermal flux boundary condition. The sinusoidal perturbation is defined by an amplitude (A) and a wavenumber (β). The effect of the larger amplitude and wavenumber is to advance the transition time, thus triggering an early onset of horizontal convection. Figure 6 shows the effect of wavenumber on the Nusselt number at $Ra = 6 \times 10^{11}$ with a perturbation amplitude of 0.01 (just 1% of the mean part of the imposed heat flux). The data demonstrates the advancement of the plume eruption phase with increasing wavenumber; $\beta = 12$ recovers an eruption time consistent with the experimentally derived data. Thus non-uniform disturbances along the heated boundary might be an explanation to the discrepancies between the numerical and experimental results. Further investigation as well as more details on the experimental set up will be needed to verify the discrepancies.

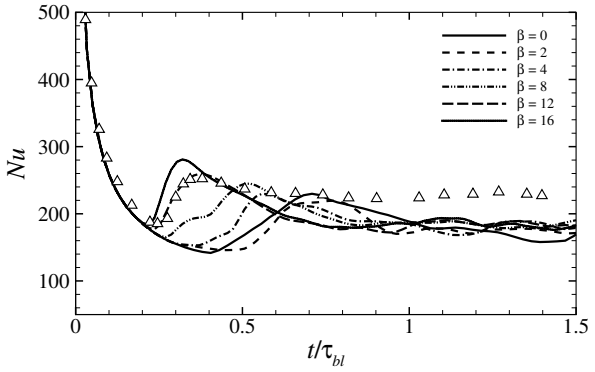

Figure 6. A plot of Nusselt number against time (scaled by the boundary layer diffusion time) for 6×10^{11} with flux amplitude of 0.01 and $\beta = 12$. Corresponding experimental data (△) from [6] are included for comparison.

Conclusions

In conclusion, the onset of horizontal convection is found to be characterised by an initial conduction phase followed by a Rayleigh–Bénard type of convection through the thermal boundary layer via multiple vertical plumes at the centre and the right end wall of the enclosure. At the onset of horizontal convection, plumes are stabilised by cooler fluid from the cold end of the enclosure, and a thermal layer begins to form and thicken. The thermal boundary layer eventually erupted and being swept toward the hot end of the enclosure, bulk overturning flows are established to form the overturning flow known to characterise horizontal convection within the enclosure.

Acknowledgements

This research was supported by Australian Research Council through Discovery Grant DP180102647, and was undertaken using high-performance computing resources from the National Computational Infrastructure (NCI) thanks to a grant under the National Computational Merit Allocation Scheme (NCMAS). NCI is supported by the Australian Government.

References

[1] Ahlers, G., Grossmann, S. and Lohse, D., Heat transfer and large scale dynamics in turbulent Rayleigh–Bénard convection, *Rev. Mod. Phys.*, **81**, 2009, 503–537.

[2] Gayen, B., Griffiths, R. W. and Hughes, G. O., Stability transitions and turbulence in horizontal convection, *J. Fluid Mech.*, **751**, 2014, 698–724.

[3] Hossain, S., Vo, T. and Sheard, G. J., Horizontal convection in shallow enclosures scales with height, not length, at low rayleigh numbers, *Int. Commun. Heat Mass*, **109**, 2019, 104308.

[4] Hughes, G. O. and Griffiths, R. W., Horizontal convection, *Annu. Rev. Fluid Mech.*, **40**, 2008, 185–208.

[5] Passaggia, P.-Y., Scotti, A. and White, B., Transition and turbulence in horizontal convection: Linear stability analysis, *J. Fluid Mech.*, **821**, 2017, 31–58.

[6] Sanmiguel Vila, C., Discetti, S., Carlomagno, G. M., Astarita, T. and Ianiro, A., On the onset of horizontal convection, *Int. J. Therm. Sci.*, **110**, 2016, 96–108.

[7] Sheard, G. J., Hussam, W. K. and Tsai, T., Linear stability and energetics of rotating radial horizontal convection, *J. Fluid Mech.*, **795**, 2016, 1–35.

[8] Shishkina, O., Grossmann, S. and Lohse, D., Heat and momentum transport scalings in horizontal convection, *Geophys. Res. Lett.*, **43**, 2016, 1219–1225.

[9] Tsai, T., Hussam, W. K., Fouras, A. and Sheard, G. J., The origin of instability in enclosed horizontally driven convection, *Int. J. Heat Mass Tran.*, **94**, 2016, 509–515.

[10] Tsai, T., Hussam, W. K., King, M. P. and Sheard, G. J., Transitions and scaling in horizontal convection driven by different temperature profiles, *Int. J. Therm. Sci.*, **148**, 2020, 106166.